REPORT DOCUMENTATION PAGE

Form Approved
OMB No. 0704-0188

1. REPORT DATE *(DD-MM-YYYY)*	**2. REPORT TYPE**	**3. DATES COVERED** *(From - To)*
22-09-2020	Interim Journal Article	01 OCT 2019 – 22 SEP 2020

4. TITLE AND SUBTITLE
Evaluation of the potential eye hazard at visible wavelengths of the supercontinuum generated by an ultrafast NIR laser in water

5a. CONTRACT NUMBER
FA8650-149-P-6074

5b. GRANT NUMBER

5c. PROGRAM ELEMENT NUMBER

6. AUTHOR(S)
Xomalin G. Peralta, Joseph E. Clary, Amanda M. Peterson, Gary D. Noojin,

Brian J. Lund, Francesco J. Echeverria, Benjamin A. Rockwell

5d. PROJECT NUMBER

5e. TASK NUMBER

5f. WORK UNIT NUMBER
H10F

7. PERFORMING ORGANIZATION NAME(S) AND ADDRESS(ES)
SAIC Inc.
4141 Petroleum Rd
JBSA Fort Sam Houston TX

8. PERFORMING ORGANIZATION REPORT NUMBER

9. SPONSORING / MONITORING AGENCY NAME(S) AND ADDRESS(ES)
Air Force Research Laboratory
711th Human Performance Wing
Airman Systems Directorate
Bioeffects Division
Optical Radiation Bioeffects Branch
4141 Petroleum Rd
JBSA Fort Sam Houston TX

10. SPONSOR/MONITOR'S ACRONYM(S)

11. SPONSOR/MONITOR'S REPORT NUMBER(S)
AFRL-RH-FS-JA-2020-0001

12. DISTRIBUTION / AVAILABILITY STATEMENT
Distribution Statement A. Approved for public release; distribution is unlimited. TSRL-PA-2020-0196. The opinions expressed on this document, electronic or otherwise, are solely those of the author(s). They do not represent an endorsement by or the views of the United States Air Force, the Department of Defense, or the United States Government.

13. SUPPLEMENTARY NOTES

14. Abstract
Lasers with ultrashort pulse durations have become ubiquitous in various applications, including ocular surgery. Therefore, we need to consider the role of nonlinear optical effects, such as supercontinuum generation during propagation within the ocular media, when evaluating their potential hazard. We used a NIR femtosecond laser to generate a supercontinuum within an artificial eye. We recorded the visible spectra of the supercontinuum generated and calculated the energy contained within the visible band. Our results indicate that for wavelengths between 1350 nm and 1450 nm the energy contained within the visible band of the generated white light supercontinuum may surpass current safety exposure limits, and pose a risk of injury to the retina.

15. SUBJECT TERMS
Eye hazard, supercontinuum, ultrafast NIR laser

16. SECURITY CLASSIFICATION OF:			**17. LIMITATION OF ABSTRACT**	**18. NUMBER OF PAGES**	**19a. NAME OF RESPONSIBLE PERSON**
a. REPORT	**b. ABSTRACT**	**c. THIS PAGE**			Dr. Joel Bixler
U	U	U	SAR Unclassified	14	**19b. TELEPHONE NUMBER** *(include area code)* 210-539-8172

Research Article | Vol. 12, No. 2 / 1 February 2021 / Biomedical Optics Express 1167
Biomedical Optics EXPRESS

Evaluation of the potential eye hazard at visible wavelengths of the supercontinuum generated by an ultrafast NIR laser in water

XOMALIN G. PERALTA,[1] JOSEPH E. CLARY,[1] AMANDA M. PETERSON,[1] GARY D. NOOJIN,[1] BRIAN J. LUND,[1] FRANCESCO J. ECHEVERRIA,[2] AND BENJAMIN A. ROCKWELL[2,*]

[1]SAIC, 4141 Petroleum Rd., JBSA Fort Sam Houston, TX 78234, USA
[2]Air Force Research Laboratory, 711th Human Performance Wing, Airman Systems Directorate, Bioeffects Division, Optical Radiation Bioeffects Branch, 4141 Petroleum Rd., JBSA Fort Sam Houston, TX 78234, USA
*Benjamin.Rockwell@us.af.mil

Abstract: Lasers with ultrashort pulse durations have become ubiquitous in various applications, including ocular surgery. Therefore, we need to consider the role of nonlinear optical effects, such as supercontinuum generation during propagation within the ocular media, when evaluating their potential hazard. We used a NIR femtosecond laser to generate a supercontinuum within an artificial eye. We recorded the visible spectra of the supercontinuum generated and calculated the energy contained within the visible band. Our results indicate that for wavelengths between 1350 nm and 1450 nm the energy contained within the visible band of the generated white light supercontinuum may surpass current safety exposure limits, and pose a risk of injury to the retina.

1. Introduction

In recent years, pulsed lasers with ultrashort pulse durations, i.e. shorter than 10 ps, have become ubiquitous in various applications [1–5] including medical procedures such as laser eye surgery [6–8]. The peak power of these sources is sufficiently high that the role of nonlinear optical effects resulting from the interaction of ultrashort pulses with the surrounding media needs to be considered when evaluating their potential hazard to the retina [9,10].

Ocular laser safety standards define the maximum permissible exposure (MPE) that can enter the eye for a specific wavelength, beam size, and exposure duration [11–13]. Current laser safety standards, such as the American National Standard for Safe Use of Lasers (ANSI Z136.1-2014) [11], the International Electrotechnical Commission for safety of laser products (IEC 60825-1:2014) [12], and the International Commission for Non-Ionizing Radiation Protection (ICNIRP) guidelines [13], include MPE limits for wavelengths ranging from 400 nm up to 1400 nm with pulse durations longer than 100 fs. The majority of the retinal threshold studies used to establish the current MPEs have used data from *in vivo* studies on non-human primates [14–17]. For wavelengths longer than 1400 nm and pulse durations shorter than 1 ns, no exposure limits are provided due to lack of biological data, but the recommendation is to use the MPE applicable to 1 ns pulse durations [11]. These standards tacitly assume that there is only linear optical propagation of light within the ocular media; therefore, the wavelength of the incoming laser beam remains unchanged as it propagates through the eye. However, there have been various studies demonstrating nonlinear optical effects in water resulting from the interaction with ultrashort pulses which lead to the generation of wavelengths other than the incoming wavelength [18–25]. One such nonlinear effect is the generation of supercontinuum (SC) light, i.e. ultra-broadband radiation with a high power spectral density and a high degree of spatial coherence [26]. The precise physical processes involved in producing the spectral broadening of the incoming laser

#415044 https://doi.org/10.1364/BOE.415044
Journal © 2021 Received 16 Nov 2020; revised 28 Dec 2020; accepted 14 Jan 2021; published 1 Feb 2021

Biomedical Optics EXPRESS

pulses depend on the specific refractive index dispersion in the material as well as pulse duration, power, and wavelength of the incident beam [27]. In particular, for femtosecond pulse durations in water, self-phase modulation, self-focusing and solitons dominate the generation of the SC [19,27,28]. The interplay between the different nonlinear effects involved results in a threshold pulse energy for the incoming beam, above which SC generation is observed [28–30]. Given that the generated SC travels in the same direction as the incoming beam [27], and the main component of the vitreous humor is water, these studies underscore the need to evaluate whether or not the SC generated by femtosecond pulses in ocular media poses a hazard to the human eye, specifically, the retina [23–25].

The near infrared (NIR) region of the electromagnetic spectrum is of particular interest from a laser safety standpoint because it includes a region of strong water absorption above 1064 nm where light propagates in an anomalous dispersion regime [19,22,31]. In addition, as the wavelength increases from 1200 to 1400 nm, due to the optical properties and absorption characteristics of the tissues, there is a gradual transition in which tissue is most sensitive to laser damage. For wavelengths in the visible range and up to ~1064 nm the damage threshold for the retina is less than that for the cornea, however, above 1400 nm the damage threshold for the cornea dominates [32–34] defining the transitional NIR region. In this study, we used a NIR femtosecond laser at wavelengths between 800 nm and 1500 nm to determine the threshold energy needed to generate a SC within a water-filled artificial eye. The artificial eye was designed to emulate the path length and focusing geometry of a non-human primate eye and was inspired by previous studies [35]. By comparing the SC generation threshold energies with the laser safety limits at NIR wavelengths, we identified wavelengths with incident energies below the laser safety limits. We recorded the visible spectra of the SC generated by the NIR wavelengths of interest at two different pulse energies and, by comparing with the spectra of a known tungsten-halogen source, calculated the energy contained within the visible band. Subsequently, we compared the SC energy generated within the visible band to the maximum permissible energy derived from the ANSI Z136.1-2014 MPE limits for visible wavelengths in order to determine if there was a potential for the corresponding exposure conditions to cause damage to the eye. These results increase our current understanding of nonlinear optical hazards associated with NIR ultrashort pulsed lasers, guide future *in vivo* experiments to establish ocular damage thresholds from SC generated by NIR ultrafast lasers, and contribute to the knowledge base used for setting laser safety standards in the transitional NIR region for ocular exposure to ultrashort pulses.

2. Methods

2.1. Supercontinuum generation

2.1.1. Optical setup for supercontinuum generation

An optical parametric amplifier (OPA; HE-TOPAS, Light Conversion Technologies) pumped by a Ti:Sapphire regenerative amplifier (Spitfire Ace, Spectra Physics) was used to produce excitation wavelengths between 800 nm and 1500 nm with a 1 kHz repetition rate and a nominal pulse duration of 100 fs. As shown in Fig. 1, we sent the output from the OPA through a set of neutral density filters to control the pulse energy and a telescope to reduce the approximately 8 mm diameter beam to a collimated 3 to 4 mm diameter beam. For wavelengths above 900 nm, we used an 850 nm long-pass filter to block any residual light from the 800 nm pump beam and any visible light components produced by the NIR light generation in the OPA. The collimated NIR light at a 1 kHz repetition rate was directed into an artificial eye that consisted of a focusing lens and a flat window at opposite ends of a water-filled container as detailed in section 2.1.2.

The SC light generated exited through the back window of the artificial eye and was collected by a Spectralon coated, 38.1 mm diameter integrating sphere with a 9.5 mm sample port opening (FOIS-1 Integrating Sphere, Ocean Insight). Using an optical fiber, we sent the output of the

Biomedical Optics EXPRESS

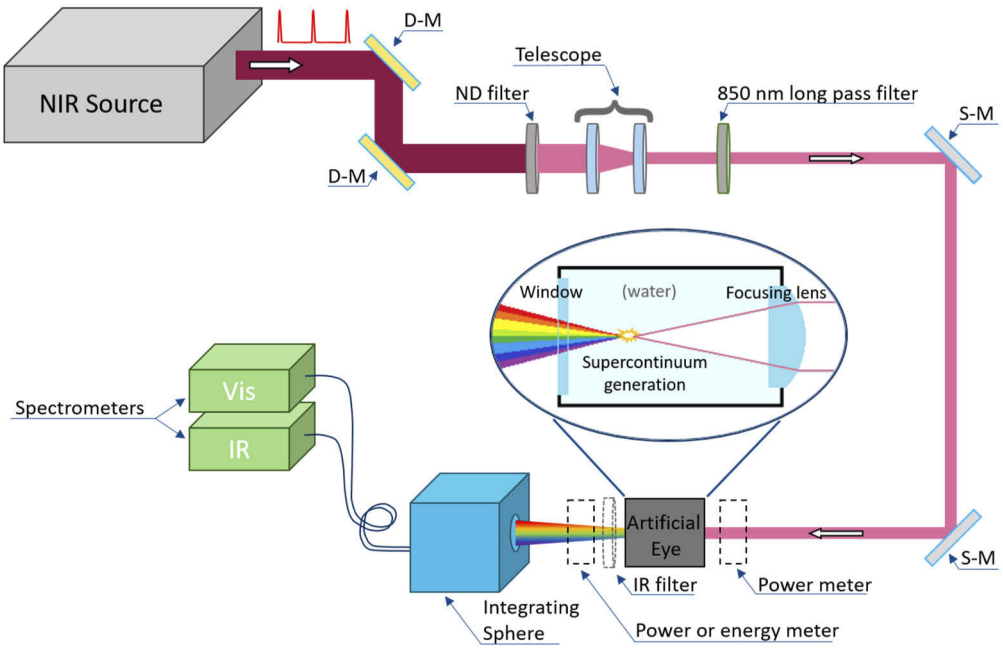

Fig. 1. Diagram of the optical setup used to measure the SC generation by an ultrafast NIR laser source. Power or energy meters and the IR short-pass filter (dotted lines) were set in place or removed depending on the type of measurement – see text. D-M: Dielectric mirror. ND: Neutral density filter. S-M: Silver mirror. Inset: Schematic diagram of SC generation within the artificial eye.

integrating sphere to a visible light spectrometer (USB 2000, Ocean Optics) or a NIR spectrometer (NIR 512, Ocean Optics) in order to capture the SC spectra in the visible and IR ranges separately. The spectra were continuously collected for specific integration times and were averaged by the spectrometer's software. For some measurements, we placed a short-pass filter (FF01-890/SP-25, Semrock) before the integrating sphere. This filter passed wavelengths between 370 nm and 875 nm, essentially blocking any UV and NIR components present in the light exiting the artificial eye and enabling us to isolate the contribution from the visible range, i.e. 380 to 740 nm, through our subsequent numerical analysis of the SC spectra. We used a power meter to measure the energy of the incoming NIR beam (PM10, Coherent) and an energy meter (J-10MB-LE, Coherent) or a power meter (919P-003-10, Ophir) to obtain the energy contained in the outgoing SC light depending on its magnitude. We built an enclosure with an opening for the NIR beam around the artificial eye and the integrating sphere to prevent ambient room light from being collected during spectral and energy measurements as determined by the suppression of the fluorescent light peaks in the visible spectrum.

We characterized the incoming NIR laser beam by measuring the IR spectrum with the NIR spectrometer and collecting the beam profile using an infrared camera (Pyrocam-III, Spiricon) right before the artificial eye. For all wavelengths used, the beam was approximately Gaussian. We calculated the diameter of the incident beam at the $1/e^2$ intensity point by averaging two separate knife-edge measurements 19 cm before and 19 cm after the artificial eye's position along the optical path when no artificial eye was present. The diameter of the beam depended on the wavelength and on the precise alignment of the telescope, varying between 2.65 mm at 1350 nm and 4.14 mm at 1400 nm.

Biomedical Optics EXPRESS

2.1.2. Artificial eye design

We designed the artificial eye to emulate the optical path length and focusing geometry of a living eye, specifically that of a non-human primate, while allowing access to light traveling to the back of the eye. It consisted of a focusing lens and a flat exit window at opposite ends of a 30 mm x 50 mm x 55 mm tall container filled with distilled water as shown in Fig. 2(a). The eye of a non-human primate has an effective focal length of 17 mm in water [36] (13.5 mm in air [37]) so the lens was selected to have a similar focal length in water which resulted in a nominal back focal length of 17.98 mm at 800 nm and 18.32 mm at 1450 nm.

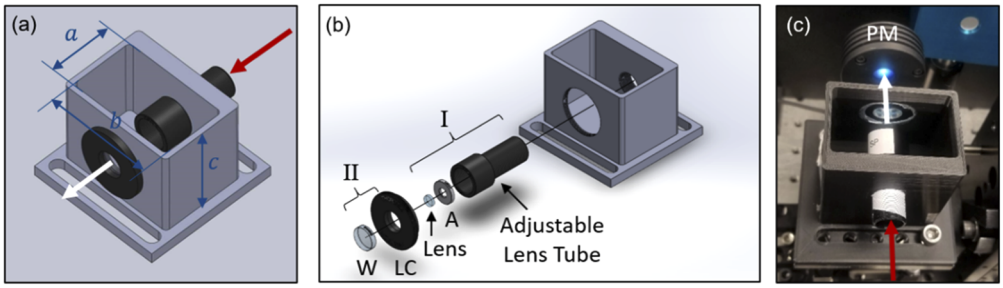

Fig. 2. (a) Mechanical drawing of the artificial eye (isometric view) showing the direction of the incoming NIR beam (red arrow) and the SC generated (white arrow). $a = 30$ mm, $b = 50$ mm, $c = 55$ mm. (b) Exploded diagram of the artificial eye. W: Infrasil exit window. LC: Lens tube cap. A: Lens holder adaptor. Roman numerals indicate independent assemblies. (c) Optical image of the artificial eye showing a real-color image of the SC generated with an incident wavelength of 1300 nm. Red arrow – incoming NIR beam. White arrow – SC generated. PM: Power meter.

The container was 3D printed out of Tough PLA (Ultimaker S5, Ultimaker B.V.) before threading the two openings on opposing sides to hold the optical components, see Fig. 2(b). The opening for the incoming NIR beam held an 8 mm diameter plano convex lens, f = 15 mm (SLB-08-15P, Opto Sigma) mounted onto a lens holder adaptor (LMRA8, Thorlabs) within a 12.7 mm diameter adjustable lens tube (SM05V10, Thorlabs), assembly I in Fig. 2(b). The opening for the outgoing generated SC held a 25.4 mm diameter lens tube cap (SM1CP2M, Thorlabs) machined to mount the 12.7 mm diameter, 1 mm thick Infrasil exit window (UDP05, Thorlabs), labeled as assembly II in Fig. 2(b). The exit window had a relatively flat spectral response and high transmission at both visible and IR wavelengths. The artificial eye was mounted on a multi-directional positioning stage (TTR001, Thorlabs) in order to facilitate the alignment of its optical axis to the laser path. The plano convex lens focused the incoming NIR light to a point within the water-filled container; furthermore, the artificial eye's design allowed for adjustments of the focal plane relative to the exit window by changing the amount the adjustable lens tube protruded into the artificial eye's chamber. The distance between the back plane of the lens and the front plane of the exit window was set at the beginning of the study and remained fixed at approximately 24 mm, leaving about 6 mm between the focal point and the front face of the exit window. Note that the exact separation depended on the wavelength of the incoming beam due to chromatic focal shift. Figure 2(c) is an optical image (real-color) of the artificial eye showing the SC generated at an incident wavelength of 1300 nm as a white-blueish light within the aperture of the power meter approximately centered in the upper half of the picture. The red and white arrows indicate the beam paths of the incoming NIR ultrafast laser pulses and the generated SC respectively.

Biomedical Optics EXPRESS

2.1.3. Determination of the threshold energy for supercontinuum generation

In order to find the threshold energy (E_{Th}) for SC generation at each NIR wavelength selected, we systematically varied the power of the incoming beam with a set of neutral density filters while monitoring the SC spectra with the visible spectrometer. Once we could resolve a clear spectrum above the noise floor, we obtained the incoming pulse energy by placing a power meter in front of the artificial eye and dividing the measured (average) power by the repetition rate of the laser and labeled it the E_{Th}. Subsequently, we removed the power meter and recorded the visible spectrum directly, the visible spectrum with the short-pass filter before the integrating sphere, and the IR spectrum. For each spectrum measured, we collected the corresponding dark spectrum by blocking the incoming NIR beam with a mechanical shutter. We then replaced the integrating sphere with an energy meter and recorded the energy in the generated SC with the short-pass filter in place. Note that at some incoming wavelengths, we could visually distinguish SC being generated at energies lower than the nominal threshold energy but were unable to measure a spectrum because it was below the sensitivity of our detection system. Similarly, for some incoming wavelengths, the energy of the generated SC with the short-pass filter in place was below the detection limit of our detectors although we could record a spectrum.

2.2. Quantification of the supercontinuum's energy contained in the visible range

In our study, the detection system consisted of the exit window of the artificial eye, the short-pass filter (if in place), the integrating sphere, the optical fiber, and the visible spectrometer. The wavelength dependent response of the detection system altered all measured spectra. To correct for this effect, we followed standard procedures used in the spectroscopy and radiometry communities [38–41]. Briefly, these procedures consist of utilizing a known broadband source to obtain the instrument response function (*IRF*) and then using the *IRF* to correct the shape and amplitude of the measured spectra. In our case, we used a tungsten-halogen broadband source (LS-1, Ocean Optics) and we obtained the *IRF* of the broadband source–exit window–integrating sphere–optical fiber–spectrometer combination. Subsequently, we corrected the SC spectrum collected with the visible spectrometer for the effect of the detection system as follows:

$$\mathrm{corr}SC(\lambda) = \frac{SC(\lambda)}{IRF(\lambda)} \tag{1}$$

where *SC* was the spectrum of the SC corrected for the transmission spectrum of the exit window and includes the respective dark spectrum, i.e. the spectrum collected with the light source blocked, and the *IRF* was obtained following standard procedures.

The energy of the SC generated within the visible range was obtained from

$$\text{Energy of SC in visible range} = \varepsilon \int_{\lambda_1}^{\lambda_2} \mathrm{corr}SC(\lambda)\, d\lambda \tag{2}$$

where the energy calibration factor (ε) is a scalar quantity that relates the intensity counts of the visible spectrometer to the energy contained in the spectrum of a known source, in this case the tungsten-halogen lamp, and the integration limits λ_1=*380 nm* and λ_2=*740 nm* correspond to the visible range of the electromagnetic spectrum. The energy calibration factor was given by

$$\varepsilon = \frac{\textit{Measured lamp's energy with filter}}{\int_{\lambda_3}^{\lambda_4} \mathrm{corr}S_F(\lambda) d\lambda} \tag{3}$$

where the lamp's output energy was measured with the short-pass filter in place in Joules and the denominator was in counts. The integrand of the denominator ($\mathrm{corr}S_F$) represents the scaled shape-corrected source's spectrum measured with the short-pass filter in place and includes the

Biomedical Optics EXPRESS

corresponding dark spectrum while the integration limits λ_3=*370 nm* and λ_4=*875 nm* correspond to the wavelength range of the short-pass filter. Note that the wavelength range of the filter encompasses the visible range, reducing any ambiguities introduced by having contributions from wavelengths outside the range of interest when calculating the energy in the visible range of the generated SC. All numerical integrations were calculated in Matlab and utilize the trapezoidal method with unit spacing.

3. Results

3.1. Determination of NIR wavelengths of interest

Table 1 lists the threshold energies determined for SC generation in the artificial eye for all the NIR wavelengths tested. In addition, it lists the Maximum Permissible Exposure limits obtained from the ANSI Z136.1-2014 corresponding to the incoming NIR wavelengths (MPE_{NIR}) selected and the corresponding maximum permissible energy, or Total Intraocular Energy (TIE_{NIR}), calculated assuming a 7 mm diameter measurement aperture [11]. Given that we have nominally 100 fs long pulses at a repetition rate of 1 kHz, we used the MPE_{NIR} values for single-pulse exposures per guidance. The last column of Table 1 lists the ratio of the threshold pulse energy to the maximum permissible energy where a ratio of less than 1 means that the incident pulse energy needed to generate SC light for that wavelength was lower than the corresponding TIE_{NIR}, therefore that incident pulse energy is considered safe per current laser safety standards. This ratio was used to determine the wavelengths of interest to be examined further in order to determine if the generated SC contained enough energy at visible wavelengths to potentially cause damage to the retina by overcoming the laser safety limits for visible wavelength. We chose to examine wavelength and energy combinations for which the ratio was less than 10, meaning that the incident pulse energy was less than ten times the corresponding maximum permissible energy, which directed our subsequent analysis to 1350 nm and longer wavelengths. At 1475 nm and 1500 nm, we observed relatively weak third harmonic generation and were unable to deliver enough energy to generate a SC. Consequently, we did not include them in any subsequent analysis or discussion.

Table 1. Threshold Energies for SC Generation and the MPE at NIR Wavelengths

Wavelength (nm)	Threshold Pulse Energy (μJ)	MPE_{NIR}[a] (J/cm^2)	TIE_{NIR}[b] (μJ)	Threshold Pulse Energy / TIE_{NIR}
800	13	1.0×10^{-7}	0.04	~300
900	5.68	1.0×10^{-7}	0.04	~150
1000	7.3	1.0×10^{-7}	0.04	~200
1120	16	1.0×10^{-7}	0.04	~400
1200	26	8.0×10^{-7}	0.31	~100
1225	3	8.1×10^{-7}	0.31	~10
1250	27.1	9.0×10^{-7}	0.35	~100
1275	29.7	1.8×10^{-6}	0.70	~50
1300	84	1.1×10^{-5}	4.16	~20
1325	347	1.0×10^{-4}	38.8	~10
1350	233	1.0×10^{-3}	385	0.6
1375	450	1.0×10^{-2}	3,850	0.12
1400	343	0.3	115,450	0.003
1435	333	0.3	115,450	0.003
1450	780	0.3	115,450	0.007

[a]The MPE_{NIR} is for single 100 fs long pulses. [b]Total Intraocular Energy corresponding to the MPE_{NIR}.

Biomedical Optics EXPRESS

Table 2 lists suprathreshold pulse energies which were all less than 2.5 times the respective E_{Th} and, except for 1350 nm, would be considered safe given that they were lower than the TIE_{NIR} corresponding to the MPE_{NIR}, i.e. the ratio of the incident pulse energy to the maximum permissible energy was less than 1 (last column in Table 2). These additional energies have been included to enable a more complete discussion of the role that the incident pulse energy has on the spectrum of the SC generated and its potential to cause damage to the retina by overcoming the laser safety limits for visible wavelengths.

Table 2. Suprathreshold Energies Tested for SC Generation

Wavelength (nm)	Incident Pulse Energy (μJ)	MPE_{NIR}[a] (J/cm^2)	TIE_{NIR}[b] (μJ)	Incident Pulse Energy / TIE_{NIR}
1350	575	1.0×10^{-3}	385	1.49
1375	800	1.0×10^{-2}	3,850	0.21
1400	475	0.3	115,450	0.004
1435	637	0.3	115,450	0.006
1450	1290	0.3	115,450	0.011

[a]The MPE_{NIR} is for single 100 fs long pulses. [b]Total Intraocular Energy corresponding to the MPE_{NIR}.

3.2. *Supercontinuum spectra at wavelengths of interest*

Figure 3 shows the energy spectra of the SC generated by the NIR wavelengths of interest. We obtained the spectra from the corrected visible SC spectrum (corr*SC*) by multiplying Eq. (1) in section 2.2 by the corresponding energy calibration factor. The black lines correspond to the E_{Th} listed in Table 1 and, for 1350 nm and 1400 nm, have been magnified fifty times. The light blue lines correspond to the suprathreshold energies listed in Table 2. The dashed vertical lines indicate the region used to determine the energy within the visible range while the dash-dotted vertical line is located at the third harmonic of the incoming beam's wavelength. The insets show the spectra of the incoming beam (dotted lines) and the IR spectra of the SC generated (solid lines) between 860 nm and 1660 nm. Table 3 lists the position of the maximal peaks in the visible and IR ranges as well as the limits of the spectral bandwidths of the SC generated for the selected exposure conditions, where the shaded rows correspond to suprathreshold energies.

Table 3. Characteristics of the SC Spectra

Wavelength (nm)	Incident Pulse Energy (μJ)	Visible SC Peak Position (nm)	Visible SC Range (nm)	IR SC Peak Position (nm)	IR SC Range (nm)
1350	233	381	340 – 530	1301	870 – 1395
1350	575	468	340 – 680	1308	860 – 1405
1375	450	418	340 – 540	1308	1030 – 1390
1375	800	500	340 – 770	1301	860 – 1395
1400	343	382	350 – 460	1282	1030 – 1390
1400	475	531	340 – 740	1268	860 – 1390
1435	333	466	400 – 840	1295	940 – 1375
1435	637	470	400 – 840	1288	860 – 1375
1450	780	478	390 – 540	1294	1020 – 1385
1450	1290	478	390 – 840	1288	860 – 1380

In the visible range, the SC spectra were all blue-shifted relative to the wavelength of the incoming beam and had bandwidths spanning between 110 nm and 450 nm. In addition, we

Biomedical Optics EXPRESS

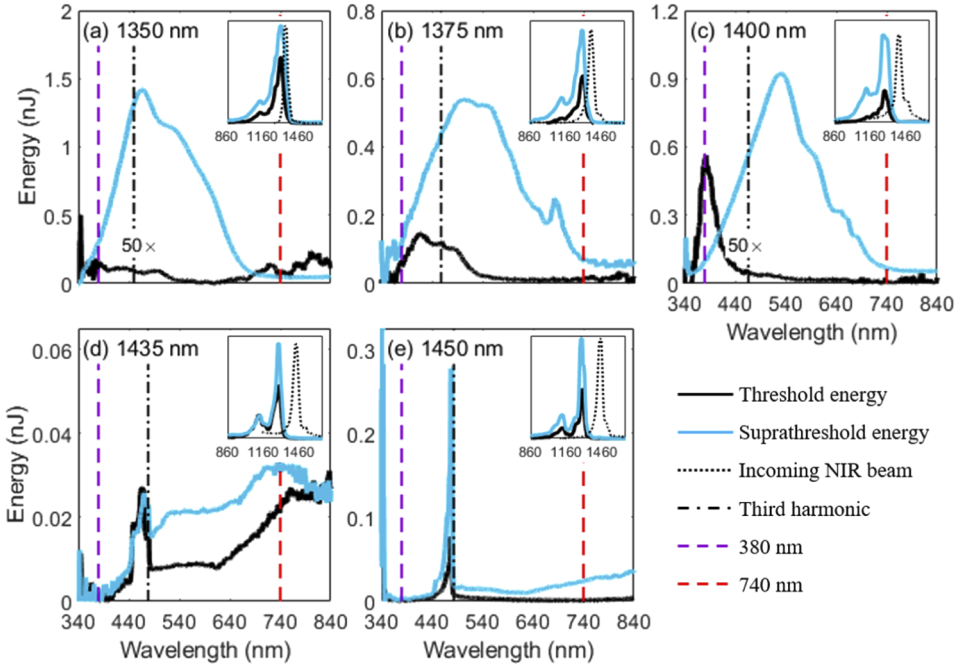

Fig. 3. (a - e) Energy spectra of the SC generated by NIR wavelengths of interest. Black lines – E_{Th} from Table 1. Light blue lines – suprathreshold energies from Table 2. Dashed lines demarcate the visible range. Dash-dotted lines indicate the third harmonic of the incoming wavelength. Insets: IR spectra of the generated SC (solid lines) and NIR incoming beam (dotted lines).

observed a redshift in the peak of the SC spectrum for 1350, 1375, and 1400 nm as the incident pulse energy was increased. At 1350 nm, the amplitude of the spectrum at E_{Th} was small and relatively featureless (black line in Fig. 3(a)). Increasing the incoming pulse energy to $2.5 \times E_{Th}$ resulted in the development of a clear peak 450 times larger in amplitude and an increase in bandwidth of ~100% relative to the spectra at E_{Th}, while remaining within 50% of the maximum permissible energy (light blue line in Fig. 3(a)). At 1375 nm, the peak amplitude of the SC spectrum increased by a factor of ~4 while the bandwidth increased ~100% when increasing the incident pulse energy to $1.7 \times E_{th}$ (Fig. 3(b)). Similarly, at 1400 nm, increasing the incident pulse energy to $1.4 \times E_{Th}$ resulted in an increase of 80 times in the peak amplitude as well as a ~4 times increase in bandwidth of the SC spectrum (Fig. 3(c)). These data demonstrate a rapid increase in the amplitude, bandwidth and spectral distribution of the generated SC as the incoming pulse energy is increased above E_{th} [42].

For 1350, 1375, and 1400 nm, the peaks in the amplitude did not appear to correspond to the third harmonic of the incoming wavelength. However, for E_{Th} at 1375 nm there was a small inflexion point in the spectrum close to the third harmonic (Fig. 3(b)), which was absent at 1350 nm and 1400 nm. For 1435 nm and 1450 nm, the spectra for third harmonic generation was superimposed on a broad spectral background (Fig. 3(d) and (e)). As the incident pulse energy was increased, the amplitude of the broad spectral background increased, confirming that it originated from the generation of a SC. At 1435 nm, the peak amplitude of the third harmonic generation did not significantly increase when the incoming pulse energy increased to $2 \times E_{Th}$ (Fig. 3(d)). However, at 1450 nm it increased ~4 times when the energy of the incoming beam increased to $1.7 \times E_{Th}$ (Fig. 3(e)).

Biomedical Optics EXPRESS

In the IR range, all the SC spectra showed significant broadening when compared to the incoming beam, see insets in Fig. 3. The bandwidths of the SC generated varied from about 360 nm for E_{Th} at 1375, 1400, and 1450 nm to a maximum of 545 nm for the suprathreshold energy at 1350 nm. All IR SC spectra had two blue-shifted peaks relative to the incoming wavelength, with the ones for 1435 nm and 1450 nm separated by a deeper trough. The peak occurring at shorter wavelengths in the IR range was located at (1130 ± 6.6) nm for all incoming wavelengths, where the uncertainty was determined by the wavelength resolution of the IR spectrometer.

3.3. *Comparison of the energy of the generated supercontinuum contained within the visible range and the maximum permissible energy at visible wavelengths*

The primary purpose of this study was to determine if the SC generated by NIR wavelengths with incident energies below the laser safety limits contained enough energy in the visible range to overcome the laser safety limits for visible wavelengths. The set of exposure conditions of interest consisted of incident NIR wavelengths with pulse energies below 10 times the maximum permissible energy obtained from laser safety standards and capable of generating a SC. Results are summarized in Table 4 where the first and second columns list the incident NIR wavelengths and pulse energies used. The third column lists the ratio of the incident pulse energy to the TIE_{NIR} corresponding to the MPE_{NIR} from column 5 in Tables 1 and 2, where a value smaller than 1 means that the incoming pulse energy was lower than the corresponding TIE_{NIR} and would be considered safe by the current standard. With the exception of 1350 nm with an incident pulse energy of 575 μJ, all other conditions fell within this category. The shaded rows in Table 4 correspond to incoming suprathreshold pulse energies.

Table 4. Comparison of the Energy of the Generated SC within the Visible Range and the Maximum Permissible Energy at Visible Wavelengths

Wavelength (nm)	Incident Pulse Energy (μJ)	Incident Pulse Energy / TIE_{NIR}	SC Energy in Visible Range (nJ)	SC Energy in Visible Range / Maximum Permissible Energy for Visible Wavelengths[a]
1350	233	0.6	3.4 ± 0.5	0.09
1350	575	1.49	698 ± 99	18.1
1375	450	0.12	66.4 ± 9.4	1.72
1375	800	0.21	468 ± 66	12.2
1400	343	0.003	1.2 ± 0.2	0.03
1400	475	0.004	451 ± 64	11.7
1435	333	0.003	30.7 ± 4.4	0.80
1435	637	0.006	54.5 ± 7.7	1.42
1450	780	0.007	4.7 ± 0.7	0.12
1450	1290	0.011	32.1 ± 4.5	0.83

[a]Maximum permissible energy at visible wavelengths is 38.48 nJ.

In order to decide if the SC generated by a set of exposure conditions posed a risk to the retina, we first had to determine how much energy was contained within the visible range. We calculated the energy of the SC generated within the visible range from the corresponding spectra using Eq. (2) in section 2.2. Results are listed in Table 4, column 4 where the uncertainty includes a 10% variability in the spectrum of the SC generated as well as the uncertainty in the determination of the *IRF* and the ε due to the source's variability. To validate these results, we compared them to the corresponding energy measurements of the SC generated with the short-pass filter at the output of the artificial eye and found that they compared favorably (data not shown). Subsequently we compared the energy of the SC generated within the visible range to

Biomedical Optics EXPRESS

the maximum permissible energy for visible wavelengths obtained from the MPE values listed in the laser safety standards for a 7 mm diameter measurement aperture. The MPE limit is constant throughout the visible range at 100 nJ/cm^2 therefore the corresponding maximum permissible energy for visible wavelengths is 38.48 nJ. The last column in Table 4 shows the result of this comparison where ratios larger than 1 indicate that the energy of the SC generated contained within the visible range of the electromagnetic spectrum is larger than the maximum permissible energy at visible wavelengths in current laser safety standards. Note that, although the MPE limits we are using are defined at specifics wavelengths, they establish a limit on the maximum permissible energy, or TIE, deposited on the retina that will not cause damage. Given that the SC generated contains a range of wavelengths, in order to avoid any confusion with the usual interpretation of the TIE for laser sources, which assume a single wavelength, we will continue using the term maximum permissible energy for visible wavelengths.

From Table 4, it can be seen that at 1350 nm, when the incoming pulse energy was approximately $^2/_3$ of the corresponding TIE_{NIR}, the energy of the SC generated within the visible range was an order of magnitude smaller than the maximum permissible energy for visible wavelengths. However, when the incident pulse energy was 50% larger than the NIR maximum permissible energy, the energy of the SC generated within the visible range was ~20 times the maximum permissible energy in the visible range. If, for simplicity, we assume a linear relationship between the incoming pulse energy and the energy of the SC generated within the visible range, we can use our results to estimate the energy of the SC generated at the corresponding TIE_{NIR} by interpolation. In particular, at the TIE_{NIR} corresponding to the MPE for 1350 nm, the energy of the SC generated within the visible range would be about 10 times the maximum permissible energy in the visible range. In contrast, at E_{Th} for 1375 nm, the incoming pulse energy was about one tenth of the corresponding TIE_{NIR} while the energy of the SC generated within the visible range was about 2 times the maximum permissible energy in the visible range. Increasing the incident pulse energy by 80%, while still almost 5 times smaller than the NIR maximum permissible energy, resulted in an increase in the energy of the generated SC within the visible range by a factor of 7, which is 12 times the maximum permissible energy in the visible range.

At 1400 nm, the energy of the generated SC within the visible range at the E_{Th}, which was about 300 times smaller than the corresponding TIE_{NIR}, was about 30 times smaller than the maximum permissible energy for visible wavelengths. However, when the incident pulse energy increased by about 40%, although it was still ~250 times smaller than the NIR maximum permissible energy, the energy of the SC generated within the visible range surpassed the maximum permissible energy allowed for visible wavelengths by more than a factor of 10. For the E_{Th} at 1435 nm, the incident pulse energy was ~300 times smaller than the corresponding TIE_{NIR} and the generated SC's energy within the visible range was ~80% of the maximum permissible energy allowed for visible wavelengths. When the incident pulse energy was increased by a factor of 2, although it was still ~160 times lower than the corresponding TIE_{NIR}, the energy of the generated SC contained within the visible range surpassed the maximum permissible energy in the visible range by ~40%. In the case of 1450 nm, the energy of the generated SC contained in the visible range at the E_{Th} was around one tenth of the maximum permissible energy allowed for visible wavelengths although the incident pulse energy was ~140 times smaller than the TIE_{NIR}. When the energy of the incident beam increased by 70%, the energy contained in the visible range of the SC generated was ~80% of the maximum permissible energy allowed for visible wavelengths.

4. Discussion

The spectra for the SC generated in this study presented similar characteristics to those found in the literature for comparable incoming wavelengths in water [19–21,24]. For 1350, 1375, and 1400 nm incident wavelengths, the visible spectra for the SC generated with the higher incident pulse energies had a distinct peak that did not correspond to the third harmonic of the incoming

Biomedical Optics EXPRESS

beam, are all somewhat asymmetric, and had spectral bandwidths of 340, 430, and 400 nm respectively. In contrast, at 1435 nm and 1450 nm, the visible spectra had a sharp peak that corresponds to the third harmonic superimposed on a broad spectral background that we attribute to SC generation. The cause of these differences in the spectral distribution may be the increase in linear absorption of water for wavelengths above 1400 nm and the relatively long water path for these experiments; ~18 mm for the incident NIR beam and ~6 mm for the generated SC. Our results were also in agreement with previous reports where a relatively modest increase in the incoming beam's energy results in a large increase in the amplitude, bandwidth and spectral distribution of the SC generated [24,43].

The primary goal of this study was to determine if the SC generated by NIR wavelengths with incident energies below the laser safety limits contain enough energy in the visible range to overcome the laser safety limits for visible wavelengths. With the exception of 1350 nm with an incident pulse energy of 575 μJ, all the incoming pulse energies for the wavelengths of interest were lower than the TIE_{NIR} corresponding to the MPE_{NIR} and would be considered safe according to current laser safety standards. More so for incoming wavelengths above 1375 nm where all of the incoming pulse energies were at least ~100 times smaller than the corresponding NIR maximum permissible energy. However, our results for suprathreshold energies showed that the energy of the SC generated within the visible range, surpassed the maximum permissible energy allowed for visible wavelengths by at least a factor of 10 for 1350, 1375, and 1400 nm while the incident pulse energy remained within 50% of the corresponding TIE_{NIR}. For 1435 nm, when the incident pulse energy was 0.6% of the NIR maximum permissible energy, the energy of the SC generated contained within the visible range surpassed the maximum permissible energy in the visible range by 40%. On the other hand, when the incident pulse energy was 1% of the NIR maximum permissible energy at 1450 nm, the highest energy available with our laser system, the energy contained in the visible range of the SC generated was ~20% below the maximum permissible energy for the visible range. Therefore, for all wavelengths of interest except 1450 nm, the energy contained within the visible range of the generated SC surpassed the maximum permissible energy allowed for visible wavelengths by the laser safety standards for the eye for at least one of the two energy conditions tested. These results agree qualitatively with recent modeling predictions [23,25].

The experiments and analysis presented in this manuscript focused on quantifying the energy of the generated SC contained within the visible range and comparing it to the maximum permissible energy at visible wavelengths obtained from laser safety standards. Laser safety standards define MPE limits for specifics wavelengths; however, the generated SC has components in the NIR in addition to the ones in the visible range that may contribute to the retinal hazard. Furthermore, laser safety standards establish a TIE corresponding to the MPE at a particular wavelength yet the generated SC contains a range of wavelengths all of which contribute to the amount of energy deposited on to the retina. These factors should be considered when designing and interpreting results from *in vivo* experiments [44]. In addition, our experiments and analysis do not take into account the effects of scattering and Fresnel reflection losses at the surface of the cornea [45,46] on the process of SC generation and, consequently, how they may affect the potential hazard the generated SC presents to the retina. Recently, there have been reports that the addition of salts increases the SC signal relative to that of pure water [47] while the addition of proteins suppresses the SC generation [48,49]. The vitreous humor contains both salts and proteins therefore it is unclear how their apparently competing contributions would impact the SC generation in a more realistic fluid model although the n_2 value for vitreous was measured to be experimentally equivalent to water [50]. In spite of these caveats, our results provide a baseline for pure water and strongly suggest that the SC generated by femtosecond pulses may pose a hazard to the human eye, highlighting the need for further studies.

Biomedical Optics EXPRESS

5. Summary

In this study, we used a NIR femtosecond laser at wavelengths between 800 nm and 1500 nm to determine the energy threshold for SC generation within a water-filled artificial eye. The artificial eye consisted of a focusing lens and a flat exit window at opposite ends of a container filled with distilled water, emulating the path length and focusing geometry of a non-human primate's eye. We found that the energy threshold for SC generation is only lower than the maximum permissible energy for wavelengths between 1350 nm and 1450 nm, where the linear absorption of water is high. We recorded the visible spectra of the SC generated at the threshold energy and a slightly higher pulse energy. By comparing with the spectra of a known tungsten-halogen source, we calculated the energy contained within the visible band. Our results indicate that for 1350 nm and longer incident wavelengths, the energy of the generated SC contained within the visible range can surpass the maximum permissible energy allowed for visible wavelengths by the laser safety standards, while remaining within the safety standards for NIR wavelengths. Notably, although the incident pulse energy was less than six thousandths of the maximum permissible energy at 1400 nm and 1435 nm, the energy of the generated SC was at least 40% higher than the maximum permissible energy at visible wavelengths. These observations indicate there is a strong potential for some exposure conditions to cause damage to the eye, not necessarily because of the incoming exposure conditions, but because of the SC generated by nonlinear effects in the aqueous media of the eye. Therefore, our results highlight the need to perform *in vivo* studies to directly evaluate potential damage to the retina from SC generated by ultrashort pulses at 1350 nm and longer wavelengths, and to validate or recommend changes to the laser safety limits for ultrashort pulsed lasers at 1400 nm and longer wavelengths.

Funding. Air Force Research Laboratory (FA8650-19-C-6204).

Acknowledgments. We would like to acknowledge Mr. Kurt J. Schuster for confirming the MPE calculations.

Disclosures. The authors declare no conflicts of interest.

References

1. W. Sibbett, A. A. Lagatsky, and C. T. A. Brown, "The development and application of femtosecond laser systems," Opt. Express **20**(7), 6989–7001 (2012).
2. National Academies of Sciences, Engineering, and Medicine, Opportunities in Intense Ultrafast Lasers: Reaching for the Brightest Light (2017).
3. M. E. Fermann, A. Galvanaukas, and G. Sucha, "Ultrafast Lasers: Technology and Applications," https://www.crcpress.com/Ultrafast-Lasers-Technology-and-Applications/Fermann-Galvanauskas-Sucha/p/book/9780367446963.
4. S. Nolte, F. Schrempel, and F. Dausinger, eds., *Ultrashort Pulse Laser Technology: Laser Sources and Applications,* Springer Series in Optical Sciences (Springer International Publishing, 2016), Vol. 195.
5. K. Sugioka and Y. Cheng, "Ultrafast lasers—reliable tools for advanced materials processing," Light: Sci. Appl. **3**(4), e149 (2014).
6. H. Lubatschowski, A. Heisterkamp, F. Will, A. Singh, J. Serbin, A. Ostendorf, O. Kermani, R. Heermann, H. Welling, and W. Ertmer, "Medical applications for ultrafast laser pulses," in RIKEN Review No. 50, (January, 2003): Focused on Laser Precision Microfabrication (2003).
7. Y. T.-Y. Lau, K. C. Shih, R. H.-K. Tse, T. C.-Y. Chan, and V. Jhanji, "Comparison of visual, refractive and ocular surface outcomes between small incision lenticule extraction and laser-assisted in situ keratomileusis for myopia and myopic astigmatism," Ophthalmol. Ther. **8**(3), 373–386 (2019).
8. H. W. Roberts, A. C. Day, and D. P. O'Brart, "Femtosecond laser–assisted cataract surgery: A review," Eur. J. Ophthalmol. **30**(3), 417–429 (2020).
9. R. W. Boyd, *Nonlinear Optics*, 3rd ed. (Academic Press, Inc., 2008).
10. J.-C. Diels and W. Rudolph, *Ultrashort Laser Pulse Phenomena: Fundamentals, Techniques, and Applications on a Femtosecond Time Scale* (Academic Press, 1996).
11. American National Standards Institute, *ANSI Z136.1-2014 American National Standard for Safe Use of Lasers* (Laser Institute of America, 2014).
12. International Electrotechnical Comission, *IEC 60825-1:2014 Safety of Laser Products - Part 1: Equipment Classification and Requirements* (International Electrotechnical Commission, 2014).
13. International Non-Ionizing Radiation Committee of the International Radiation Protection Association, "Guidelines on limits of exposure to laser radiation of wavelengths between 180 nm and 1 mm," Health Phys **49**, 341–359 (1985).

Biomedical Optics EXPRESS

14. B. E. Stuck, "Ocular susceptibility to laser radiation: human vs. rhesus monkeys," in *Handbook of Laser Bioeffects Assesment* (Letterman Army Institute of Research, 1984), Vol. 1, pp. 67–83.
15. International Commission on Non-Ionizing Radiation Protection, "ICNIRP Guidelines on Limits of Exposure to Laser Radiation of Wavelengths between 180 nm and 1,000 μm," Health Phys **105**(3), 271–295 (2013).
16. D. J. Lund and B. J. Lund, "The determination of laser-induced retinal injury thresholds," ILSC **2015**, 69–73 (2015).
17. D. H. Sliney, A. Robinson, and S. Sparks, Laser Hazards Bibliography, January 1991 (Army Environmental Hygiene Agency Aberdeen Proving Ground Md, 1991).
18. G. Mao, Y. Wu, and K. D. Singer, "Third harmonic generation in self-focused filaments in liquids," Opt. Express **15**(8), 4857–4862 (2007).
19. P. Vasa, J. A. Dharmadhikari, A. K. Dharmadhikari, R. Sharma, M. Singh, and D. Mathur, "Supercontinuum generation in water by intense, femtosecond laser pulses under anomalous chromatic dispersion," Phys. Rev. A **89**(4), 043834 (2014).
20. F. J. Echeverria, "Nonlinear optical effects on retinal damage thresholds in the 1200-1400 nm wavelength range," Thesis (2015).
21. F. Echeverria, B. Hokr, J. Bixler, A. Sokolov, M. Schmidt, G. Noojin, R. Thomas, and B. Rockwell, "Nonlinear optical effects and trends of near-infrared laser retinal damage," ILSC **2015**, 63–65 (2015) .
22. J. A. Dharmadhikari, G. Steinmeyer, G. Gopakumar, D. Mathur, and A. K. Dharmadhikari, "Femtosecond supercontinuum generation in water in the vicinity of absorption bands," Opt. Lett. **41**(15), 3475–3478 (2016).
23. C. Marble, V. V. Yakovlev, and A. W. Wharmby, "Simulated supercontinuum generation in water and the human eye," in *Nonlinear Frequency Generation and Conversion: Materials and Devices XVIII*, P. G. Schunemann and K. L. Schepler, eds. (SPIE, 2019), p. 30.
24. A. R. Boretsky, J. E. Clary, G. D. Noojin, D. J. Burner, and B. A. Rockwell, "Non-linear optical hazards from near-infrared ultrafast laser pulses in ocular tissue," ILSC **2019** 301 (2019) .
25. C. Marble and A. W. Wharmby, Simulated Supercontinuum Generation in the Human Eye from 1200 Nm to 1400 Nm, Air Force Technical Report AFRL-RH-FS-TR-2018-0025 (2018).
26. A. Dubietis, A. Couairon, and G. Genty, "Supercontinuum generation: introduction," J. Opt. Soc. Am. B **36**(2), SG1 (2019).
27. R. R. Alfano, ed., *The Supercontinuum Laser Source* (Springer-Verlag, 1989).
28. P. Vasa, M. Singh, R. Bernard, A. K. Dharmadhikari, J. A. Dharmadhikari, and D. Mathur, "Supercontinuum generation in water doped with gold nanoparticles," Appl. Phys. Lett. **103**(11), 111109 (2013).
29. A. Dubietis and A. Couairon, *Ultrafast Supercontinuum Generation in Transparent Solid-State Media* (Springer, 2019).
30. P. B. Corkum, C. Rolland, and T. Srinivasan-Rao, "Supercontinuum generation in gases," Phys. Rev. Lett. **57**(18), 2268–2271 (1986).
31. C. Marble, J. Clary, G. Noojin, S. O'Connor, D. Nodurft, A. Wharmby, B. Rockwell, M. Scully, and V. Yakovlev, "Z-scan measurements of water from 1150 to 1400 nm," Opt. Lett. **43**(17), 4196 (2018).
32. J. A. Zuclich, D. J. Lund, and B. E. Stuck, "Wavelength dependence of ocular damage thresholds in the near-IR to far-IR transition region: proposed revisions to MPES," Health Phys. **92**(1), 15–23 (2007).
33. D. J. Lund, P. R. Edsall, D. R. Fuller, and S. W. Hoxie, "Bioeffects of near-infrared lasers," J. Laser Appl. **10**(3), 140–143 (1998).
34. H. Chen, Z. Yang, J. Wang, P. Chen, and H. Qian, "A comparative study on ocular damage induced by 1319 nm laser radiation: Ocular damage induced by near infrared lasers," Lasers Surg. Med. **43**(4), 306–312 (2011).
35. C. Cain, G. Noojin, D. Hammer, R. Thomas, and B. Rockwell, "Artificial eye for in vitro experiments of laser light interaction with aqueous media," J. Biomed. Opt. **2**(1), 88–94 (1997).
36. Y. Qiao-Grider, L.-F. Hung, C. Kee, R. Ramamirtham, and E. L. Smith, "Normal ocular development in young rhesus monkeys (Macaca mulatta)," Vision Res. **47**(11), 1424–1444 (2007).
37. R. J. Clarke, H. Zhang, and P. D. R. Gamlin, "Characteristics of the pupillary light reflex in the alert rhesus monkey," J. Neurophysiol. **89**(6), 3179–3189 (2003).
38. C. L. Wyatt, *Electro-Optical System Design for Information Processing, Optical and Electo-Optical Engineering Series* (Utah State University Faculty Monographs, 1991), Vol. 115.
39. Instrument Response Corrections, Technical Note 203, Optical Spectroscopy Division (Horiba Jobin Yvon, n.d.).
40. Making Measurements for Relative Irradiance, Technical Note (Ocean Optics, n.d.).
41. H. W. Yoon and C. E. Gibson, *NIST Measurement Services:: Spectral Irradiance Calibrations* (National Institute of Standards and Technology, 2011), p. NIST SP 250–89.
42. V. Jukna, N. Garejev, G. Tamošauskas, and A. Dubietis, "Role of external focusing geometry in supercontinuum generation in bulk solid-state media," J. Opt. Soc. Am. B **36**(2), A54 (2019).
43. T. S. Robinson, S. Patankar, E. Floyd, N. H. Stuart, N. Hopps, and R. A. Smith, "Spectral characterization of a supercontinuum source based on nonlinear broadening in an aqueous K_2ZnCl_4 salt solution," Appl. Opt. **56**(35), 9837 (2017).
44. L. Jiao, Y. Fan, J. Wang, and Z. Yang, "Comparative study of retinal injuries induced by a 420-750 nm supercontinuum source and a 532 nm laser," Biomed. Opt. Express **10**(6), 3018 (2019).
45. D. A. Atchinson and G. Smith, *Optics of the Human Eye* (Elsevier, 2000).

Biomedical Optics EXPRESS

46. T. J. T. P. van den Berg, "Intraocular light scatter, reflections, fluorescence and absorption: what we see in the slit lamp," Ophthalmic. Physiol. Opt. **38**(1), 6–25 (2018).
47. T. Jimbo, V. L. Caplan, Q. X. Li, Q. Z. Wang, P. P. Ho, and R. R. Alfano, "Enhancement of ultrafast supercontinuum generation in water by the addition of Zn^{2+} and K^{+} cations," Opt. Lett. **12**(7), 477–479 (1987).
48. C. Santhosh, A. K. Dharmadhikari, K. Alti, J. A. Dharmadhikari, and D. Mathur, "Suppression of ultrafast supercontinuum generation in a salivary protein," J. Biomed. Opt. **12**(2), 020510 (2007).
49. C. Santhosh, A. K. Dharmadhikari, J. A. Dharmadhikari, K. Alti, and D. Mathur, "Supercontinuum generation in macromolecular media," Appl. Phys. B **99**(3), 427–432 (2010).
50. B. A. Rockwell, C. P. Cain, G. D. Noojin, W. P. Roach, M. E. Rogers, M. W. Mayo, and C. A. Toth, "Nonlinear refraction in vitreous humor," Opt. Lett. **18**(21), 1792 (1993).